Distributed compressed sensing based channel estimation for underwater acoustic multiband transmissions

Yuehai Zhou,[1] Aijun Song,[2] F. Tong,[1,a)] and Ryan Kastner[3]
[1]*Key Laboratory of Underwater Acoustic Communication and Marine Information Technology of the Ministry of Education, Xiamen University, Xiamen, Fujian 361005, China*
[2]*Department of Electrical and Computer Engineering, University of Alabama, Tuscaloosa, Alabama 35487, USA*
[3]*Department of Computer Science and Engineering, University of California, San Diego, 9500 Gilman Drive, La Jolla, California 92093, USA*

(Received 4 December 2017; revised 15 May 2018; accepted 16 May 2018; published online 29 June 2018)

Distributed compressed sensing techniques are applied to enhance sparse channel estimation performance in underwater acoustic multiband systems. The core idea is to use receptions from multiple sub-bands to enhance the detection of channel tap positions. A known variant of the orthogonal matching pursuit (OMP) algorithm based on the distributed compressed sensing principle is simultaneous orthogonal matching pursuit (SOMP). However, the impulse responses across multiple sub-bands may have different arrival structures, although they often show a certain level of similarity. To address such differences at the sub-bands, a multiple selection strategy is applied to select multiple candidates at individual sub-bands at each iteration. This is different from the conventional OMP and SOMP algorithms that select only one candidate at each iteration. When the multiple selection strategy is combined with the SOMP algorithm, the proposed algorithm is referred to as JB-MSSOMP algorithm. To take advantage of channel coherence between adjacent data blocks from different sub-bands, the multiple selection strategy is further used over time. This leads to JBT-MSSOMP algorithm. Computer simulations show improved channel estimation performance of the proposed JB-MSSOMP and JBT-MSSOMP algorithms over the OMP or SOMP algorithms. Communication data from a recent acoustic experiment demonstrates improved receiver performance with the proposed channel estimators. © *2018 Acoustical Society of America*.
https://doi.org/10.1121/1.5042362

[CFM] Pages: 3985–3996

I. INTRODUCTION

Multiband transmission is an alternative strategy to orthogonal frequency division multiplexing (OFDM) or single-carrier transmissions to utilize a wide bandwidth. In this paper, we address channel estimation in underwater acoustic multiband systems. The underwater acoustic channel is typically sparse, meaning that the impulse response often has limited significant taps over the large delay spread. Compressed sensing methods are often investigated to improve the performance of channel estimation in underwater acoustic communication. We particularly apply distributed compressed sensing (DCS) techniques to enhance sparse channel estimation performance in underwater acoustic multiband systems.

In multiband transceivers, a wide frequency band is divided into multiple sub-bands that are separated by guard bands. This strategy offers a compromise between single-carrier communication and OFDM communication.[1] Multiband transmission has longer symbol duration than single-carrier transmissions, for the same bandwidth. This leads to shorter lengths of the discrete impulse responses, which in turn result in lower computational costs in channel estimation and equalization. Compared with OFDM, multiband transmissions do not suffer from the issues of high peak-to-average power ratios and sensitivity to Doppler.

Multiband transmissions have not been intensively studied in underwater acoustic communications except in a limited number of reports,[1–4] while in contrast extensive efforts have been devoted to single-carrier and OFDM communication schemes. In Roy *et al.*,[1] underwater acoustic multiband multiantenna transmissions were used in combination with multichannel decision-feedback equalization. In Walree and Leus,[2] a multicarrier spread-spectrum scheme was proposed for underwater acoustic environments, multicarrier equalizer acted as a maximal-ratio combiner that allowed for joint equalization and de-spreading. In Song and Badiey,[3] time reversal multiband acoustic communication was investigated for a frequency band of 22 kHz. In Leus and Walree,[4] a bandwidth of 3.6 kHz was divided into 16 sub-bands, each of which was modulated by OFDM. In these efforts,[1–4] the correlation of the impulse responses among sub-bands was not exploited for channel estimation.

The compressed sensing (CS) channel estimation methods have been employed to yield performance enhancement by exploitation of sparseness. For example, CS is widely used for single carrier channel estimation[5–9] and OFDM channel estimation.[10–13] However, underwater acoustic channels are characterized by substantial time variations, large spread, limited bandwidth, shorter observation lengths lead to better

a)Electronic mail: ftong@xmu.edu.cn

capability to track channel variation and improve the bandwidth efficiency. In addition, underwater acoustic channels suffer from background noise which leads to low signal-to-noise ratio (SNR). The performance of CS channel estimation will degrade under short observation lengths and low SNR.

DCS exploits multiple observed signals to enhance sparse data recovery which exhibits strong correlation from noisy measurements.[14] DCS based channel estimation has found successful applications in wireless radio-frequency communications.[15–18] Cheng *et al.*[16] introduced a novel DCS based channel estimation approach to track doubly selective channels with a large Doppler shift for OFDM system. DCS was applied to make joint sparsity channel estimation for Q order BEM coefficient vectors. A time-frequency channel estimation for multiple-input−multiple-output (MIMO)-OFDM systems under the framework of distributed compressed sensing was proposed in Ding *et al.*[18] To enhance the partially common tap delays channel estimates, a pseudorandom preamble which was identical for all transmit antennas was adopted. Then, a very small amount of pilots were used for the accurate channel recovery. Limited efforts have been reported in underwater acoustic communications that utilize DCS channel estimation. In Zhou *et al.*,[19] DCS based estimation method was developed for underwater acoustic MIMO system to suppress the co-channel interference. Two adjacent data blocks were simultaneously used to jointly estimate MIMO impulse responses. In Zhou *et al.*,[11] a DCS based channel estimation method was proposed to reduce the pilot number in underwater acoustic OFDM systems. Two adjacent data blocks in the frequency domain were combined to conduct joint sparsity channel estimation. Currently, the DCS method has not been investigated in underwater acoustic multiband transmission systems.

With a limited bandwidth up to tens of kilohertz, there exists considerable channel correlation among the sub-bands in underwater acoustic multiband systems, namely, channel delays exhibit similar structures, but channel coefficients are different. DCS based algorithms can take advantage of such correlation to improve channel estimation performance. The improvement can shorten observation lengths or enhance estimate accuracy in low SNR. A nature choice along this direction is SOMP algorithm, which uses receptions from multiple sub-bands to enhance detection channel tap positions. However, the impulse responses across multiple sub-bands may have different arrival structures, although they often show certain level of similarity. The different arrival structures will be estimated as noise.

In this paper, we applied DCS techniques to enhance sparse channel estimation for underwater acoustic multiband systems. In order to address the different arrival structures at multiple sub-bands, inspired by Kwon *et al.*[20] and Shim *et al.*,[21] we introduced a multiple selection strategy that combined with SOMP. The main idea of multiple selection strategy is that, at each SOMP iteration, every candidate generates multiple child candidates including channel delays, channel coefficients, and residual. The set of taps that minimize the overall residue are chosen as the tap positions for each sub-band. While the conventional OMP and SOMP algorithms select only one candidate at each iteration. The improved algorithm is referred to as multiple selection SOMP (MSSOMP). To take advantage of channel coherence between adjacent data blocks, we use the multiple selection strategy both over multiple sub-bands and time domain. The resultant algorithm is referred to as joint band and time sparsity multiple selection SOMP (JBT-MSSOMP) algorithm. Both computer simulations and a field experiment were conducted to show the effectiveness of the multiple selection strategy in channel estimation.

This paper is organized as follows. Section II describes the multiband system model. Section III introduces the DCS theory and formulates MSSOMP estimation schemes. Section IV analyzes the simulation results and underwater acoustic communication field experimental results are described and analyzed in Sec. V. Finally, some concluding remarks are drawn in Sec. VI. The following notations are used in this paper. Bold upper case and lower case letters denote matrices and column vectors, respectively. $\mathbf{a} \odot \mathbf{b}$ denotes the dot product of vector $\mathbf{a}$ and vector $\mathbf{b}$. Superscripts $(\cdot)^T$, $(\cdot)^H$, $(\cdot)^\dagger$ denote the transpose, Hermitian transpose and pseudo inversion operation, respectively. $\mathbf{0}_{P\times L}$ and $\mathbf{I}$ denote zero matrix with P rows and L columns, and the identity matrix, respectively. $||\cdot||_0$, $||\cdot||_1$, $||\cdot||_2$ denote the L_0 norm, L_1 norm, and Euclid norm. Matrix $\mathbf{A}[\mathbf{j}]$ denotes a sub-matrix obtained from $\mathbf{j}th$ columns of $\mathbf{A}$. Notation $\langle \mathbf{a}, \mathbf{b} \rangle$ denotes inner product of $\mathbf{a}$ and $\mathbf{b}$. $\mathbb{E}(\cdot)$ denotes the expectation operation. $\cup$ denotes the union operation. $\emptyset$ denotes the empty set. $\mathbb{C}^{M\times N}$ represents the set of $M \times N$ matrices in the complex field.

II. PROBLEM FORMULATION

We consider a single-input/multiple-output (SIMO) multiband acoustic communication system in the ocean. It is assumed that the underwater acoustic channel does not change within a limited block duration (noted as P samples), but varies with blocks. The discrete baseband receiver equation at the ith hydrophone, jth sub-band, kth block is shown as

$$y_{i,j,k}(n) = \sum_{l=0}^{L-1} x_{j,k}(n-l)h_{i,j,k}(l) + \omega_{i,j,k}(n),$$
$$i = 1,\ldots,N, j = 1,\ldots,M, k = 1,\ldots,K, \quad (1)$$

where n is the symbol index within a data block, N is the number of hydrophones, M is the total number of sub-bands, K is the total number of data blocks. $x_{j,k}(n)$ is the transmitted symbols from jth sub-band kth data block. The channel impulse response at ith hydrophone jth sub-band kth data block is described via $h_{i,j,k}(n)$, where L is the discrete channel length. The ambient noise $\omega_{i,j,k}(n)$ is additive white Gaussian distributed. Under the quasi-stationary assumption that channel remains stable within a data block of P samples, the receiver equation Eq. (1), can be presented in a matrix-vector form,

$$\mathbf{y}_{i,j,k} = \mathbf{A}_{j,k}\mathbf{h}_{i,j,k} + \boldsymbol{\omega}_{i,j,k}, \quad (2)$$

where $\mathbf{A}_{j,k}$ is a $P \times L$ Toeplitz matrix

$$\mathbf{A}_{j,k}=\begin{pmatrix} x_{j,k}(L-1) & x_{j,k}(L-2) & \cdots & x_{j,k}(0) \\ x_{j,k}(L) & x_{j,k}(L-1) & \cdots & x_{j,k}(1) \\ \vdots & \vdots & \ddots & \vdots \\ x_{j,k}(L+P-2) & x_{j,k}(L+P-3) & \cdots & x_{j,k}(P-1) \end{pmatrix}, \tag{3}$$

$$\mathbf{y}_{i,j,k}=\begin{pmatrix} y_{i,j,k}(L-1) & y_{i,j,k}(L) & \cdots & y_{i,j,k}(L+P-2) \end{pmatrix}^T, \tag{4}$$

$$\mathbf{h}_{i,j,k}=\begin{pmatrix} h_{i,j,k}(0) & h_{i,j,k}(1) & \cdots & h_{i,j,k}(L-1) \end{pmatrix}^T, \tag{5}$$

$$\boldsymbol{\omega}_{i,j,k}=\begin{pmatrix} \omega_{i,j,k}(L-1) & \omega_{i,j,k}(L) & \cdots & \omega_{i,j,k}(L+P-2) \end{pmatrix}^T. \tag{6}$$

The SIMO multiband impulse responses $\mathbf{h}_{i,j,k}$ can be estimated by the traditional LS algorithm, based on the receiver equations. The Toeplitz matrix $\mathbf{A}_{j,k}$ satisfies restricted isometry property (RIP),[22] and underwater acoustic channel is typically sparse, namely, underwater acoustic channel response has very few non-zero taps, but has a large spread delay. So, the compressed sensing can be directly utilized to estimate the underwater acoustic sparse channel.

III. DISTRIBUTED COMPRESSED SENSING ESTIMATION OF MULTIBAND TRANSMISSION CHANNEL

A. SOMP based distributed compressed sensing

For underwater acoustic multiband systems, the channels in sub-bands and data blocks have very strong correlation, it can be described by joint sparsity model 2 (JSM-2) in DCS theory.[14] In JSM-2, all the channels share the same support-set, namely, all the channels have the same tap delays, but different tap coefficients.

The SOMP algorithm has been widely used to solve JSM-2 problem.[11,15,18,19] For underwater acoustic multiband DCS channel estimation, shown as Fig. 1, the channel delays in each sub-band and each data block are the same under JSM-2 framework. The sparse channel delays can be estimated by the data from all sub-bands and from their corresponding adjacent data blocks, the channel coefficients are individually estimated based on the selected channel delays,

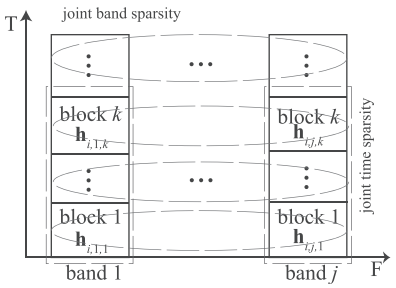

FIG. 1. Diagram of joint band sparsity and joint time sparsity channel estimation. The x axis is the frequency (sub-band index), and the y-axis is the time (data block index). Subscript (j, k) denotes the coordinate of the data block that comes from jth sub-band in frequency axis kth data block in time axis.

it is the core idea of SOMP algorithm. The way that utilizes multiple data blocks to find the same channel delays is referred as to joint sparsity estimation. As illustrated in Fig. 1, if multipath delays are jointly estimated by multiple data blocks from time axis, we denote it as joint time sparsity channel estimation which is marked with dotted rectangle. Similarly, if multipath delays are jointly estimated by the data blocks from sub-bands, we denote it as joint band sparsity channel estimation which is marked with dotted ellipse. If multipath delays are jointly estimated by the data blocks from both time and band, we denote it as joint band and time sparsity channel estimation.

Considered multiple receptions $\boldsymbol{y}_{i,j,k}$, $j=1,2,\ldots,M$, $k=1,2,\ldots,Q$ that obtained from Q adjacent data blocks from each of M sub-bands, the purpose of DCS is to simultaneously reconstruct MQ channels $\boldsymbol{h}_{i,j,k}$. Based on the concept of DCS, we establish the following model

$$\begin{pmatrix} \mathbf{y}_{i,1,1} \\ \vdots \\ \mathbf{y}_{i,M,1} \\ \vdots \\ \mathbf{y}_{i,1,Q} \\ \vdots \\ \mathbf{y}_{i,M,Q} \end{pmatrix} = \begin{pmatrix} \mathbf{A}_{1,1} & \cdots & \mathbf{0}_{P\times L} & \cdots & \mathbf{0}_{P\times L} & \cdots & \mathbf{0}_{P\times L} \\ \ddots & \ddots & \ddots & \ddots & \ddots & \ddots & \ddots \\ \mathbf{0}_{P\times L} & \cdots & \mathbf{A}_{M,1} & \cdots & \mathbf{0}_{P\times L} & \cdots & \mathbf{0}_{P\times L} \\ \ddots & \ddots & \ddots & \ddots & \ddots & \ddots & \ddots \\ \mathbf{0}_{P\times L} & \cdots & \mathbf{0}_{P\times L} & \cdots & \mathbf{A}_{1,Q} & \cdots & \mathbf{0}_{P\times L} \\ \ddots & \ddots & \ddots & \ddots & \ddots & \ddots & \ddots \\ \mathbf{0}_{P\times L} & \cdots & \mathbf{0}_{P\times L} & \cdots & \mathbf{0}_{P\times L} & \cdots & \mathbf{A}_{M,Q} \end{pmatrix} \times \begin{pmatrix} \mathbf{h}_{i,1,1} \\ \vdots \\ \mathbf{h}_{i,M,1} \\ \vdots \\ \mathbf{h}_{i,1,Q} \\ \vdots \\ \mathbf{h}_{i,M,Q} \end{pmatrix} + \begin{pmatrix} \boldsymbol{\omega}_{i,1,1} \\ \vdots \\ \boldsymbol{\omega}_{i,M,1} \\ \vdots \\ \boldsymbol{\omega}_{i,1,Q} \\ \vdots \\ \boldsymbol{\omega}_{i,M,Q} \end{pmatrix}, \tag{7}$$

$$\begin{pmatrix} \mathbf{y}_1 \\ \vdots \\ \mathbf{y}_m \\ \vdots \\ \mathbf{y}_{MQ} \end{pmatrix} = \begin{pmatrix} \mathbf{A}_1 & \cdots & \mathbf{0}_{P\times L} & \cdots & \mathbf{0}_{P\times L} \\ \ddots & \ddots & \ddots & \ddots & \ddots \\ \mathbf{0}_{P\times L} & \cdots & \mathbf{A}_m & \cdots & \mathbf{0}_{P\times L} \\ \ddots & \ddots & \ddots & \ddots & \ddots \\ \mathbf{0}_{P\times L} & \cdots & \mathbf{0}_{P\times L} & \cdots & \mathbf{A}_{MQ} \end{pmatrix} \begin{pmatrix} \mathbf{h}_1 \\ \vdots \\ \mathbf{h}_m \\ \vdots \\ \mathbf{h}_{MQ} \end{pmatrix} + \begin{pmatrix} \boldsymbol{\omega}_1 \\ \vdots \\ \boldsymbol{\omega}_m \\ \vdots \\ \boldsymbol{\omega}_{MQ} \end{pmatrix}, \tag{8}$$

$$\mathbf{Y}_i = \tilde{\mathbf{A}}\mathbf{H}_i. \tag{9}$$

To simplify the equation, we eliminate the receiving hydrophone index i, and adopt one subscript in notations instead of two. Equation (8) is the mapping of Eq. (7). The relationship between (j, k) and m is that $m = (k-1) * M + j$. In Eq. (9), $\mathbf{Y}_i \in \mathbb{C}^{QMP\times 1}$, $\tilde{\mathbf{A}} \in \mathbb{C}^{QMP\times QML}$, and $\mathbf{H}_i \in \mathbb{C}^{QML\times 1}$. The variable Q is the number of data blocks from each of M sub-bands in time domain. In Eq. (7), a comprehensive band and time sparsity with a dimension of $M * Q$ is considered. The advantage of Eq. (7) is that multiple data blocks can be used to improve the common tap delays detection, while in the OMP algorithm, only one data block is used. So the DCS has more potential to recover the underwater acoustic channels. Thus, the DCS based channel estimation can be formulated as the following optimization problem:[23,24]

$$\min\|\mathbf{Y}_i - \tilde{\mathbf{A}}\mathbf{H}_i\|_2^2 \quad s.t.\|\mathbf{h}_1\odot,\ldots,\odot\mathbf{h}_m\odot,\ldots,\odot\mathbf{h}_{MQ}\|_0 = S. \tag{10}$$

In Eq. (10), the constraint condition can be described that, all the channels contain S multipath arrivals with common delays, while the sparsity of each channel may be different. The SOMP algorithm[25] can be directly used to optimize Eq. (10). All of the received signals including different sub-bands and adjacent data blocks are jointly combined to measure the multipath delays. In this way, channels that have common delays are enhanced. When the SOMP algorithm is applied to multiband underwater acoustic channels, the algorithm is referred as to the joint band and time sparsity simultaneous orthogonal matching pursuit (JBT-SOMP). Note that when $Q = 1$, the JBT-SOMP algorithm reduces to joint band sparsity recovery noted as JB-SOMP, when both $Q = 1$ and $M = 1$, the algorithm reduces to the conventional OMP algorithm.

B. Multiple selection distributed compressed sensing

In this section, we consider the channels that not only contain common tap delays but also differential tap delays. Under time-varying and low SNR underwater acoustic channels, the multipath components with common tap delays will decrease, and that with differential tap delays increase. The channels are described as

$$\mathbf{h}_m = \mathbf{h}_m^c + \mathbf{h}_m^d, \tag{11}$$

where the superscript c and d denote the channel components with common tap delays and those with differential tap delays. The difference between Eq. (11) and JSM-2 is that, Eq. (11) contains not only the common tap delays, but also the differential tap delays. The channel estimation performance that based JSM-2 will be degraded because of loss of differential tap delays.

Previous DCS work[11,15–19] has been done based on JSM-2, but limited work for channel estimation that consider differential tap delays has been done recently. In this paper, we proposed multiple selection distributed compressed sensing for underwater acoustic multiband channels to enhance channel estimation using common tap delays and address the differential tap delays to further improve channel estimation.

For underwater acoustic multiband channel estimation, assume that M sub-bands and Q adjacent data blocks in each sub-band are combined to estimate the channels shown in Fig. 1, so there are total MQ data blocks. We apply multiple selection strategy to the SOMP algorithm to estimate the channels simultaneously. There are three kinds of candidates, channel delay candidates, coefficient candidates, and residual candidates, respectively. Each candidate generates multiple child candidates (denoted as D child candidates), which make up trees by multiple selection strategy shown in Fig. 2, this is the core idea of multiple selection. There are also three kinds of trees, delay trees, coefficient trees, and residual trees, which are composed of delay candidates, coefficient candidates, and residual candidates. The delay trees, coefficient trees, and residual trees are used to save channel delays, channel coefficients, and residual, respectively. The three kinds of trees have the same structure, shown as Fig. 2. For sth iteration (s is the iteration index), there are total D^s child candidates, which are generated from their father candidates at (s–1)th iteration, shown in Fig. 2. Each of the D^s candidates re-generates another D child

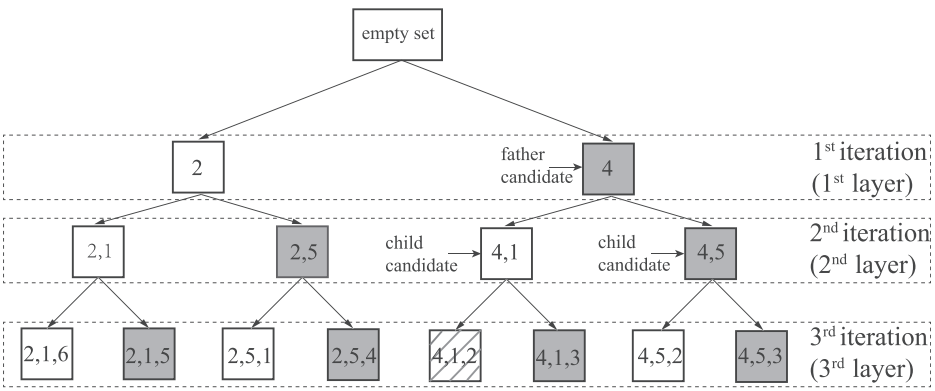

FIG. 2. The structure of one delay tree. The delay trees, coefficient trees, and the residual trees have the same structure. One square denotes a candidate, so there are delay candidates, coefficient candidates, and residual candidates. In sth iteration, the candidates are denoted as child candidates that are generated from their father candidates in $(s-1)$ th iteration. There are s elements in a candidate in sth iteration. Figure 2 shows the case where $D = 2$, $S = 3$, the information in the candidates is the channel tap delays. Compared with two child delay candidates that come from the same father delay candidate, the white delay candidate always has larger coefficient than the gray one, so the white candidate is first generated.

candidates for $(s+1)$ th iteration. At $(s+1)$ th iteration, the candidates are treated as child candidates, while the candidates from sth iteration are treated as father candidates. At the last iteration, we measure all the residual from residual candidates, and save the position that has the minimum residual. Based on the position, we select the coefficients and the channel delays from coefficient candidates and delay candidates at the last iteration. Thus the channels are constructed. The resultant algorithm is referred to as JBT-MSSOMP algorithm. When $D=1$, the JBT-MSSOMP algorithm reduces to JBT-SOMP.

The specific steps for implementing the JBT-MSSOMP algorithm are summarized as follows:

Input: received signal blocks $\mathbf{y}_m$, the measure matrix $\mathbf{A}_m$, $m=1,\ldots,MQ$, and the sparsity S.

Output: $\mathbf{h}_m$, where $m=1,\ldots,MQ$

Initialize: build MQ delay trees, coefficient trees, and residual trees, denoted as $\mathbf{\Gamma}_m$, $\boldsymbol{\rho}_m$, and $\mathbf{u}_m$, respectively, where $m=1,\ldots,MQ$. All the delay candidates, coefficient candidates, and residual candidates are set empty. Set the iteration index $s=0$. Initialize the residual $\mathbf{u}_m^0=\mathbf{y}_m$, $m=1,\ldots,MQ$. The superscript denotes the iteration number.

Iteration $s=1:S$

Sub-iteration $g^{s-1}=1:D^{s-1}$ (Note that D^{s-1} is a constant, it is not a variant.)

Step 1: measure the channel delays

$$\lambda_{g^{s-1}}=\arg\max_{q=1,\ldots,L}\sum_{m=1}^{MQ}|\langle\mathbf{A}_m[q],\mathbf{u}_m^{s-1}(g^{s-1})\rangle| \tag{12}$$

g^{s-1} denotes the candidate index in the $(s-1)$th layer in a tree. $\mathbf{u}_m^{s-1}(g^{s-1})$ denotes the g^{s-1}th residual candidate in $(s-1)$th iteration in mth residual tree. Measure inner product of $\mathbf{u}_m^{s-1}(g^{s-1})$ and $\mathbf{A}_m[q]$, where $\mathbf{A}_m[q]$ is a vector that comes from the qth column from $\mathbf{A}_m$. Add all the MQ inner products, shown as Eq. (12). Then, from the number of L added inner products, find the first D maximum values, and save their positions into $\lambda_{g^{s-1}}$. $\lambda_{g^{s-1}}$ is a scalar array, which contains number of D different potential channel delays. From Eq. (12), channel delays are determined by multiple data blocks, while in OMP algorithm, channel delays are determined by only one block. So, channels that have common delays will be enhanced by JBT-MSSOMP algorithm. In addition, in OMP or SOMP algorithm, only one delay candidate is selected, while in the JBT-MSSOMP algorithm, there are D candidates are selected which has more potential to find the correct channel delays. Step 1 can be described that one father delay candidate generates D child delay candidates.

The child candidates are extensions of their father candidates from previous iteration, and inherit the information from their father candidates, including delay candidates, coefficient candidates, and residual candidates, Fig. 2 shows the delay candidates case.

Step 2: There are D^{s-1} delay candidates in $(s-1)$ th iteration, by using multiple selection strategy in step 1, every delay candidate re-generates another D child delay candidates, so there are total $D^{s-1}*D$ delay candidates. Save the $D^{s-1}*D$ delay candidates into sth layer in delay trees, shown as Eq. (13). From Eq. (13), we can observe that, all the delay trees contain the same delay information.

$$\mathbf{\Gamma}_m^s(g^s)=\mathbf{\Gamma}_m^{s-1}(g^{s-1})\cup\boldsymbol{\lambda}_{g^{s-1}}(d)\quad d=1,\ldots,D,m=1,\ldots,MQ. \tag{13}$$

The relationship between the father candidate index g^{s-1} in $(s-1)$th iteration and the child candidate index g^s in sth iteration is $g^s=(g^{s-1}-1)D+d$, where d is the generated order of D child candidates which come from the same father candidate. For example, in Fig. 2, in the third iteration, the shadow square is first generated, and the index of its father candidates in second iteration is 3, so $g^2=3$, $d=1$. Therefore, the index of the gray square is $g^3=(g^2-1)*D+d=5$. Equation (13) demonstrates that the child delay candidates inherit the information from their father delay candidates.

Measure the coefficients, save the coefficients into coefficient candidates at sth layer in coefficient trees. Measure the residual, and save the residual into the residual candidates at sth layer in residual trees,

$$\boldsymbol{\rho}_m^s(g^s)=\mathbf{A}_m^\dagger\left[\mathbf{\Gamma}_m^s(g^s)\right]*\mathbf{y}_m,\quad m=1,\ldots,MQ. \tag{14}$$

$$\mathbf{u}_m^s(g^s)=\mathbf{y}_m-\mathbf{A}_m^\dagger\left[\mathbf{\Gamma}_m^s(g^s)\right]*\boldsymbol{\rho}_m^s(g^s),\quad m=1,\ldots,MQ. \tag{15}$$

Note that, the information in different coefficient trees is different, so is in the residual trees.

end sub-iteration

end iteration

Output: The final residual is saved in $\mathbf{u}_m^S(g^S)$, measure the minimum residual among D^S residual candidates in a tree at Sth iteration. So there are MQ minimum residual candidates that are saved,

$$\hat{g}_m^S=\underset{g^S=1:D^S}{\operatorname{argmin}}||\mathbf{u}_m^S(g^S)||_2^2,\quad m=1,\ldots,MQ. \tag{16}$$

$\hat{g}_m^S$ denotes index of the selected residual candidate that has the minimum residual at Sth layer in the mth tree. Select the coefficients in the coefficients trees and delays in the delay trees via the selected residual candidate index $\hat{g}_m^S$,

$$\hat{\mathbf{h}}_m=\boldsymbol{\rho}_m^S(\hat{g}^S{}_m),\quad m=1,\ldots,MQ. \tag{17}$$

Thus, there are total MQ channels are reconstructed, the coefficients are $\boldsymbol{\rho}_m^S(\hat{g}_m^S)$ and the tap delays are $\mathbf{\Gamma}_m^S(\hat{g}_m^S)$, where $m=1,\ldots,MQ$.

From Eq. (12), it is evident that all the delays are determined by multiple data blocks, multipath components that have common delays are enhanced, but multipath components that have differential delays will be estimated as fake taps which may have negative impact to channel equalizer. By the multiple selection strategy shown as Eqs. (14) and (15), if the differential tap delays located in the first D maximum candidates, it will be delivered to the candidates in Sth iteration. By minimizing the residue in Sth iteration shown

TABLE I. Computational complexity.

Description	Computational complexity
OMP	$\mathcal{O}(PL + Ps + Ps^2 + Ps^3)$
JBT-SOMP	$\mathcal{O}(PL + (PL + Ps + Ps^2 + Ps^3))$
JBT-MSSOMP	$\mathcal{O}(\kappa PL + \kappa D(PL + Ps + Ps^2 + Ps^3))$

in Eq. (16), both common tap delays and the differential tap delays will be selected to reconstruct the channels.

From Fig. 2, we can see that, the trees grow exponentially, when either D or the maximum iteration S is large, the computational cost will become prohibitive. So we choose a parameter κ that comprises the channel estimation performance and the computational complexity. During sth iteration, we choose the first κ maximum coefficient candidates, and their corresponding coefficient candidates and residual candidates. So during sth iteration, there are κ candidates instead of D^s candidates. Many tap delay candidates are identical because of the common tap delays. Therefore, the actual number of child candidates is often moderate. Fortunately, the acoustic channel is sparse, which means that the number of the significant taps are limited, the computational complexity of JBT-MSSOMP algorithm seems acceptable.

C. Computational complexity analysis

In this subsection, computational complexities of the OMP, JBT-SOMP, and JBT-MSSOMP algorithms are analyzed. We assume that multiplication and addition have the same computational cost.[26,27] The total complexity of the OMP algorithm is $\mathcal{O}(PL + Ps + Ps^2 + s^3)$ at the sth iteration.[26]

Table I shows the computational complexity of the OMP, JBT-SOMP, and JBT-MSSOMP algorithms at each iteration. For each channel estimate, the JBT-SOMP algorithm almost has the same complexity as the OMP algorithm. The JBT-MSSOMP algorithm has higher computational cost due to the generation of multiple child candidates. Its complexity is controlled by D and κ. Since the underwater acoustic channel is sparse, the value of κ is limited. The resultant complexity of the proposed JB-MSSOMP JBT-MSSOMP and algorithm is still acceptable.

D. Multichannel estimation based decision feedback equalization

Considered that the true underwater acoustic channel is unknown in field tests, we utilize the communication performance of multichannel estimation based decision feedback equalization (MCE-DFE) to assess the performance of channel estimators. The MCE-DFE contains a feedforward filter bank, feedback filter and a decision device. A channel convolution matrix is constructed based on channel estimates. Then the feedforward and feedback equalizer coefficients are obtained from the convolution matrix based on the minimum mean squared error criterion.[28]

IV. NUMERICAL SIMULATIONS

In this section, numerical simulations are presented to evaluate the performance of the JB-SOMP, JB-MSSOMP, and JBT-MSSOMP methods in estimation of the underwater acoustic multiband channel. A two-band underwater acoustic communication system was simulated. We utilized BELLHOP model to generate the impulse response for one sub-band, referred to as band-1. In the BELLHOP simulation, the water depth was 20 m. The sound speed was set as 1500 m/s, evenly across the water column. The depth of source was 8 m. The receiver depth was 14 m. The source−receiver range was 1000 m. The carrier frequency was set as 85 kHz. The other band, referred to as band-2, was manually generated to investigate two scenarios of multiband acoustic transmissions. In scenario I, the multiband impulse responses only contained common tap delays, as shown in Fig. 3(a). In scenario II, the impulse responses consisted both common tap delays and differential tap delays, as shown in Fig. 3(b). Specifically in Fig. 3(b), the first, third, and fourth taps of the impulse response at band-2 had different arrival times from those at band-1.

The communication simulations were carried out in the baseband. The symbol rate was 12 kilosymbol/s, and Quadrature Phase Shift Keying (QPSK) was used as the mapping scheme. The received SNR was set as 3 dB. The sparsity S in the CS and DCS algorithms was set at 7, the number of the sub-bands M was set at 2, the number of data blocks Q was set at 2. In the JB-MSSOMP and JBT-MSSOMP algorithms, κ was set at 10, the number of child candidates D was set at 5. All the parameters were chosen by tuning the mean square error (MSE) to minimum. The MSE in channel estimation is defined as

$$\gamma = 10\log_{10}\left(\frac{||\mathbf{h}_m - \hat{\mathbf{h}}_m||_2^2}{||\mathbf{h}_m||_2^2}\right), \tag{18}$$

where $\mathbf{h}_m$ is the simulated impulse response, and $\hat{\mathbf{h}}_m$ is the corresponding channel estimate.

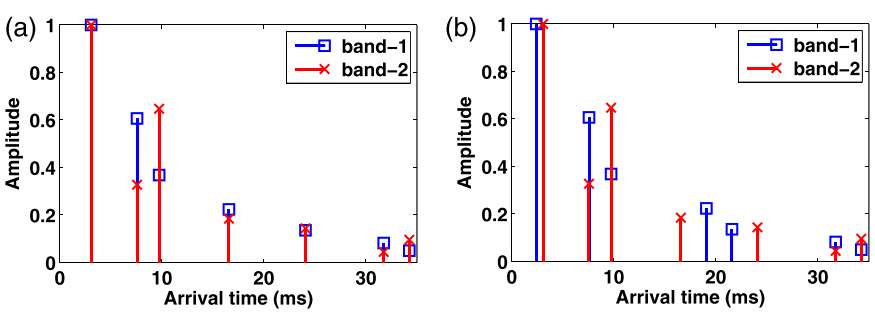

FIG. 3. (Color online) Simulation sub-band channels. (a) Sub-band channel responses with common tap delays. (b) Sub-band channel responses with partially common tap delays and partially differential tap delays.

The performance comparison for the first scenario is shown in Figs. 4(a) and 4(b) among four channel estimators: the OMP, JB-SOMP, JB-MSSOMP, and JBT-MSSOMP algorithms. Figure 4(a) shows channel estimation MSE comparison for the band-1 impulse response while Fig. 4(b) for band-2. We observe that the channel estimation MSE obtained by the JB-SOMP, JB-MSSOMP, and JBT-MSSOMP algorithms were all lower than that by OMP, indicating a better performance than the OMP algorithm. The reason is that the two sub-band impulse responses shared the common tap delays which were used to enhance channel estimation performance. The JBT-MSSOMP algorithm achieved the best performance, because the JBT-MSSOMP algorithm used the observations from both multiple sub-bands and multiple data blocks. The average MSE obtained by JBT-MSSOMP, JB-MSSOMP, and OMP algorithms in Fig. 4(a) was −12.06, −10.97, and −9.79 dB, while it was −13.20, −12.18, and −11.18 dB in Fig. 4(b). There was more than −2 dB MSE performance enhancement compared with the JBT-MSSOMP and OMP algorithms. Meanwhile, there was about −1 dB average MSE enhancement compared with the JB-MSSOMP and OMP algorithms.

Figures 4(c) and 4(d) show the channel estimation MSE for the second scenario, where the two bands shared partially common tap delays and partially differential tap delays. The MSE obtained by the JB-SOMP algorithm was lower than that of OMP under short observation lengths, for example 5−10 ms, in Figs. 4(c) and 4(d). However, in Figs. 4(c) and 4(d), with the increasing of the observation length beyond 20 ms, the JB-SOMP algorithm had slightly worse performance than the OMP algorithm, for example, when the observation length is 25 ms, the MSE obtained by the OMP and JB-SOMP algorithms in Fig. 4(c) was −12.33 and −12.10 dB, respectively. The reason is that the long observation length improves the performance of OMP algorithm, while the JB-SOMP algorithm suffers from increasing estimation noise caused by the differential tap delays at two sub-bands, shown as Eq. (11). The JB-MSSOMP and JBT-MSSOMP algorithms outperformed either the JB-SOMP or OMP algorithm, for all observation lengths shown in the plots. The performance improvements can be explained by the adoption of the multiple selection strategy to address the differential tap delays at the two sub-bands. It can be seen that the JB-SOMP and JB-MSSOMP algorithms in Fig. 4(a) did not show much performance difference. However, they had considerable differences in Fig. 4(c). The average MSE difference between the JB-SOMP and JB-MSSOMP algorithms in Fig. 4(c) were 0.76 dB. This confirmed the merit of the multiple section strategy in the second scenario.

Because of the partially shared common tap delays in the two sub-bands, the MSE obtained by the JB-MSSOMP and JBT-MSSOMP algorithms in Fig. 4(c) was slightly higher than those in Fig. 4(a). The average MSE obtained by JBT-MSSOMP in Fig. 4(c) was −11.74 dB while that in Fig. 4(a) was −12.06 dB. The comparison between Fig. 4(b) and Fig. 4(d) showed similarly small differences.

V. EXPERIMENTAL RESULTS

A. Experimental setting

To further demonstrate the effectiveness of the proposed channel estimation schemes, we used underwater acoustic communication measurements from our recent field experiment to perform channel estimation and equalization. The

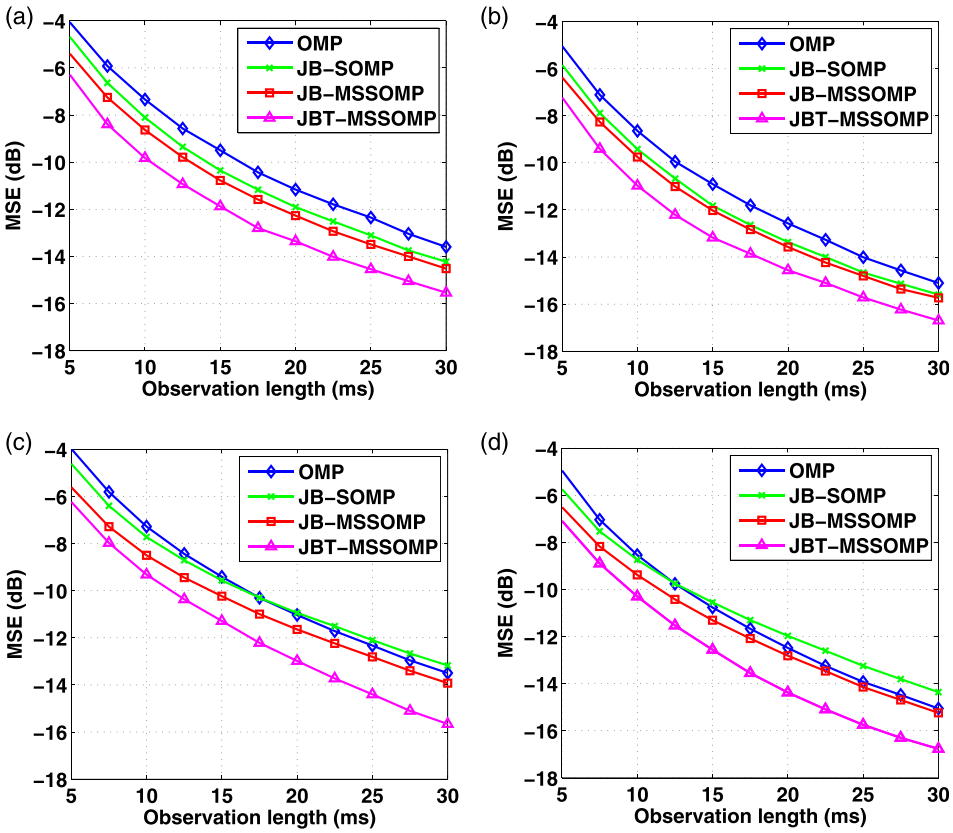

FIG. 4. (Color online) MSE versus channel observation length for (a) band-1 in scenario I. (b) band-2 in scenario I. (c) band-1 in scenario II.(d) band-2 in scenario II.

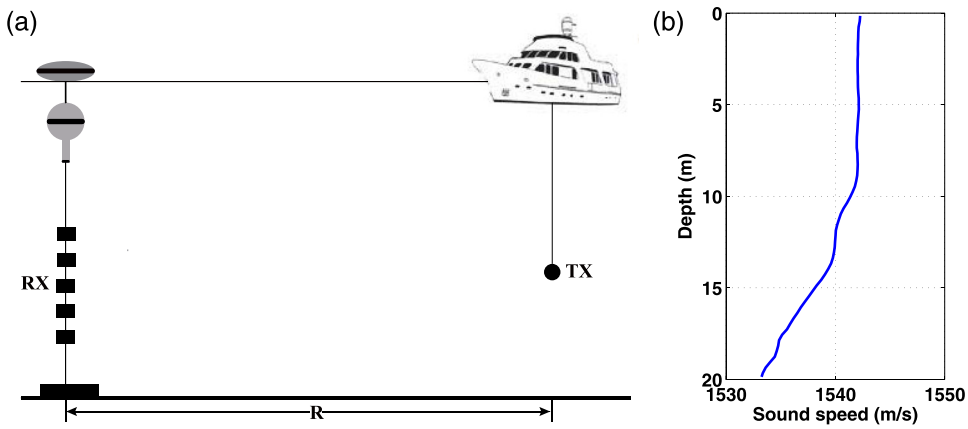

FIG. 5. (Color online) Experimental setup and sound speed profiles. (a) Experimental diagram, (b) sound speed profile.

acoustic experiment was conducted in the northern Gulf of Mexico, August 22, 2016. The water depth of the site was 20 m. A five-element broadband receiver array was deployed in a mooring, as shown in Fig. 5(a). The five-element array covered 9−16 m with an element spacing of 1.75 m. A transducer was hung from a research vessel that was anchored at different stations during the experiment. The transducer had a source level of about 177 dB re 1 μPa at 1 m. Its central frequency is 85 kHz, with a bandwidth of 20 kHz. The transducer depth was 12 m. Figure 5(b) shows the sound speed profile at the experiment site. The profile indicated a highly stratified ocean environment.

A three-band QPSK signal was transmitted during the experiment, namely, the number of the sub-bands was $M = 3$. The three sub-bands had the central frequencies of 78, 85, and 92 kHz, with 1 kHz guard band in-between, referred to as band-1, band-2, and band-3, respectively. The signal duration was 6.25 s. The symbol rate of each sub-band was 6 kilosymbol/s.

B. Channel characteristics

The average SNR of the received data obtained at the 500 and 1000 m ranges was 36.2 and 29.1 dB across the sub-bands, respectively. To demonstrate the performance of the proposed methods under low SNR regions, we added recorded noise to the original communication measurements at the 1000 m range. After noise addition, the SNR level at each sub-band was 10 dB for the 1000 m range. The resultant data is referred to as the low SNR data. The communication measurements at the 500 m range were referred to as the high SNR data. The coherence time at the 500 and 1000 m range was 241.1 and 115.5 ms, respectively. Considering the coherence time, we were able to use adjacent data blocks to perform DCS based channel estimation.

Figure 6 shows the estimated impulse responses of the middle hydrophone located at the depth of 12.5 m. The source motion generated non-negligible time-varying Doppler effects, as the source was hung from the research vessel, the average Doppler was calculated with known symbols by a narrowband iterative method[29] before channel estimation. The instantaneous Doppler reached ± 15 Hz, although the average Doppler for the packet was only a couple of hertz. We set the channel length at 33.33 ms. The channel observation length was three times of the channel length, that was 100 ms. The impulse responses were estimated by the Least Square QR-factorization (LSQR) method which is a fast algorithm of LS.

As shown in Fig. 6, the multipath energy was limited to a few channel taps, the channel impulse responses had a sparse structure. Meanwhile, there existed rich multipath arrivals that shared common tap delays [$\mathbf{h}_m^c$ in Eq. (11)] among three sub-bands. It clearly shows that there existed partially differential tap delays [$\mathbf{h}_m^d$ in Eq. (11)].

C. Communication performance in training mode

Because channel impulse response is unknown in field communication, the MCE-DFE was adopted for performance

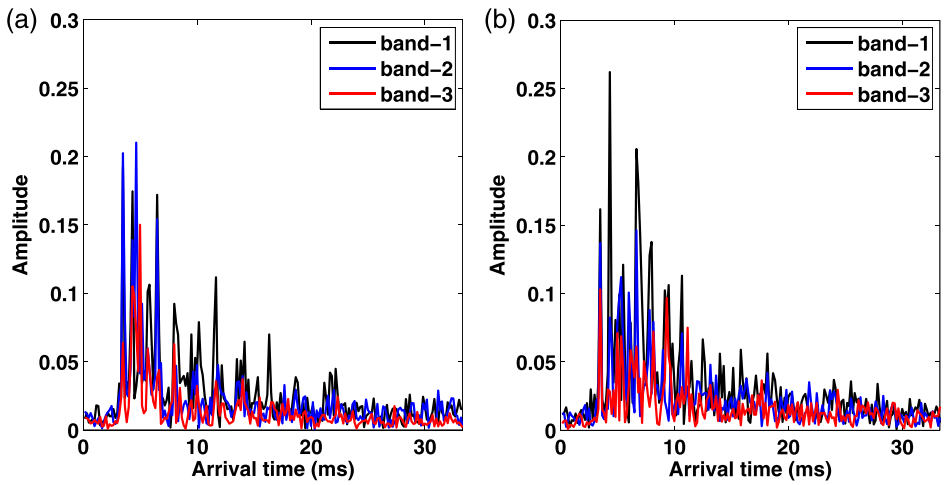

FIG. 6. (Color online) Snapshots of estimated impulse responses at the 500 m range (a) and at the 1000 m range (b), for the middle hydrophone with a depth of 12.5 m.

TABLE II. Parameters setting.

Parameters	Description	Value
Fs	Sampling frequency	510 kHz
Fc	Sub-band carrier frequency	78, 85, and 92 kHz
R	Symbol rate	6 kilosymbol/s
N_T	Number of transducers	1
N_R	Number of hydrophone channels	5
K_{os}	Over sampling factor	1
T_{preamble}	Duration of preamble	0.26 s
T_{ch}	Channel impulse response duration	33.33 ms
L	Length of discrete channel	$L = T_{\text{ch}} * R$
N_{ff}	Feedforward filter span	$2L$
N_{fb}	Feedback filter span	$L - 1$

evaluation of different algorithms in terms of the communication quality. The communication metrics were adopted to assess the performance of channel estimation algorithm: output SNR, bit error rate (BER), and the constellation. The output SNR at mth data block is defined as

$$\gamma_{\text{OSNR}} = 10\log_{10}\left(\frac{||\mathbf{x}_m||_2^2}{||\mathbf{x}_m - \hat{\mathbf{x}}_m||_2^2}\right), \tag{19}$$

where $\mathbf{x}_m$ is the transmitted symbols, and $\hat{\mathbf{x}}_m$ is the receiver soft output. Five channel estimators, including the LSQR, OMP, JB-SOMP, JB-MSSOMP, and JBT-MSSOMP algorithms, were used in the receiver.

The receiver parameters are listed in Table II. The channel length was set at $T_{\text{ch}} = 33.33$ ms, corresponding to $L = 200$ symbols. The length of feedforward filter was $N_{\text{ff}} = 2L$ symbols. The length of feedback filter was $N_{fb} = L - 1$ symbols. In the OMP, JB-SOMP, JB-MSSOMP, and JBT-MSSOMP algorithms, the sparsity was set at 30. In the JB-MSSOMP and JBT-MSSOMP algorithms, κ was set at 10, and the number of child candidates in Eq. (12) was set at $D = 5$, it is a compromise between computation complexity and performance. Two adjacent data blocks were used for joint channel estimation in the JBT-MSSOMP algorithm, i.e., $Q = 2$.

In the training mode, channel estimators assumed perfect knowledge of the transmitted symbols. Figure 8 shows the receiver output SNR in the training mode from band-1. In both Figs. 7(a) and 7(b), the output SNR increased with the increased channel observation length for each of the channel estimation algorithms. Clearly, the LSQR algorithm resulted in the worst performance. Among the OMP, JB-SOMP, JB-MSSOMP, and JBT-MSSOMP algorithms, the proposed JB-MSSOMP and JBT-MSSOMP algorithms achieved higher output SNR under short observation length, for example less than 20 ms. At the observation length of 13.33 ms, the JB-MSSOMP and JBT-MSSOMP algorithms resulted in 1.57 and 2.45 dB gain over the OMP algorithm in Fig. 7(a). Their gains were 1.17 and 2.12 dB in Fig. 7(b) for the same observation length of 13.33 ms. The JB-SOMP algorithm had slightly better performance than the OMP algorithm in both plots. The JBT-MSSOMP algorithm achieved the higher gain when the observation length was short, less than 20 ms.

In the high SNR case shown in Fig. 7(a), the output SNR of CS and DCS channel estimators converged when the observation length was larger than 25 ms. In the high SNR scenario, with a large channel observation length, the DCS methods did not have performance advantages. In the low SNR case [Fig. 7(b)], the JB-MSSOMP and JBT-MSSOMP algorithms still led to some performance advantages over the OMP algorithms at the channel observation length of 26.67 ms. Their gains were 0.67 and 1.29 dB over the OMP algorithm.

We further analyze the channel estimation performance under different sparsity. Specially, in this part, we compare the performance of JBT-SOMP algorithm. For the receiver parameters, the observation length is fixed at 13.33 ms, the remaining parameters are the same as previous settings in the training mode. LSQR, OMP, JB-SOMP, JB-MSSOMP, JBT-SOMP, and JBT-MSSOMP algorithms are compared under different sparsity.

From Fig. 8, it can be observed that, the output SNR obtained by OMP, JB-SOMP, JB-MSSOMP, JBT-SOMP, and JBT-MSSOMP algorithms varied with sparsity, while the output SNR obtained by LSQR algorithm kept constant. It is evident that, the JBT-MSSOMP channel estimator obtained the best performance both in Figs. 8(a) and in 8(b).

In Fig. 8, the output SNR obtained by OMP algorithm decreased when the sparsity increased. In Fig. 8(a), the JBT-MSSOMP channel estimator obtained the maximum output SNR 10.12 dB at the sparsity of 25, the JB-SOMP, JB-MSSOMP, and JBT-SOMP channel estimator obtained the

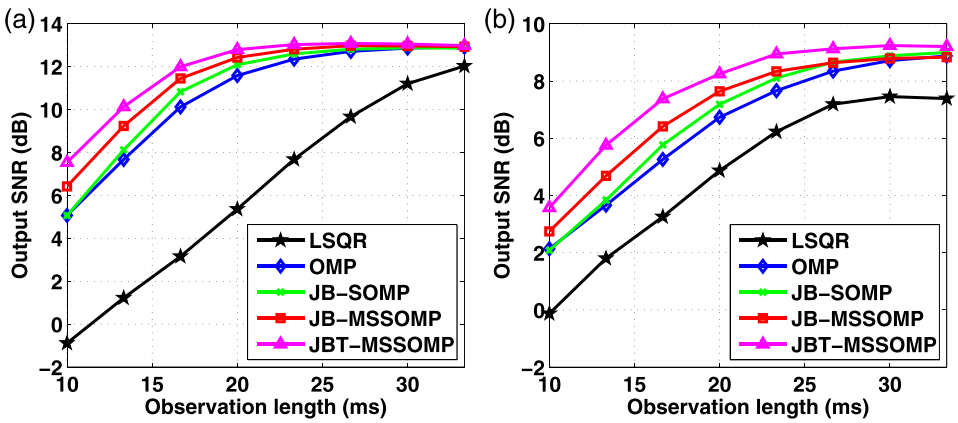

FIG. 7. (Color online) Output SNR versus channel observation length for the high SNR data (a) and for the low SNR data (b), at band-1. Note that the y-axis limits in (a) and (b) are 14 and 10 dB.

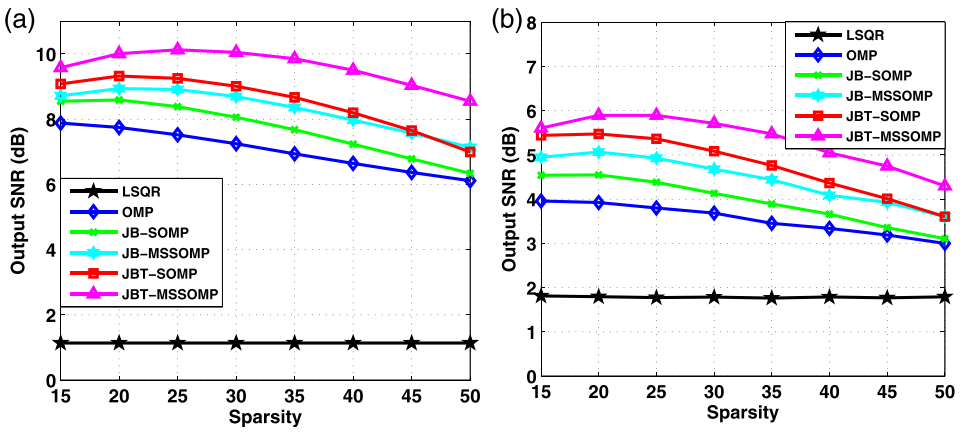

FIG. 8. (Color online) Output SNR versus sparsity for the high SNR data (a) and for the low SNR data (b) at band-1.

maximum output SNR at the sparsity of 20, the output SNR was 8.59, 8.94 and 9.32 dB, respectively. In Fig. 8(b), The JBT-MSSOMP, JB-MSSOMP, and JB-SOMP algorithms obtained the best output SNR at the sparsity of 20. Note that, both in Figs. 8(a) and 8(b), when the sparsity was 50, the output SNR obtained by OMP and JB-SOMP algorithms was closed, while the JB-MSSOMP and JBT-MSSOMP algorithms still achieved high gains, because the JB-MSSOMP and JBT-MSSOMP algorithms applied multiple selection strategy. Compared with JBT-SOMP and JB-MSSOMP algorithms in both Figs. 8(b) and 8(a), we can see that, when the sparsity was less than 40, the output SNR obtained by JBT-SOMP was larger than that obtained by JB-MSSOMP. When the sparsity was 50, the performance between JBT-SOMP and JB-MSSOMP was very closed.

D. Performance in decision-directed mode

In the decision-directed mode, the previous detected symbols were used in both channel estimation and Doppler estimation. A 0.26 s preamble was used to estimate the initial channel impulse responses and Doppler estimates. Four channel estimators, OMP, JB-SOMP, JB-MSSOMP, and JBT-MSSOMP, were considered in the decision-directed mode. The parameters of MCE-DFE receiver were set the same as in the training mode listed in Table II. The parameters in OMP, JB-SOMP, JB-MSSOMP, and JBT-MSSOMP algorithms were also set the same as in the training mode. Periodic training was adopted to prevent error propagation. The periodical training symbols accounted for 14.29% of the transmitted symbols.

The channel observation length was $P = 100$ symbols (16.67 ms) in Fig. 9(a) and $P = 160$ symbols (26.67 ms) in Fig. 9(b). In Fig. 9(a), the OMP, JB-SOMP, JB-MSSOMP, and JBT-MSSOMP achieved the output SNR of 4.85, 6.09, 7.61, and 8.96 dB. In Fig. 9(b), the OMP, JB-SOMP, JB-MSSOMP, and JBT-MSSOMP algorithm achieved the output SNR of 4.13, 4.81, 5.38, and 5.95 dB. The output SNR achieved by the JB-MSSOMP and JBT-MSSOMP algorithms resulted in better performance than the conventional OMP. The JBT-MSSOMP algorithm achieved the highest output SNR. The comparison results in the decision-directed mode were consistent with those in the training mode. The output SNR associated with the OMP algorithm showed an oscillation feature because of the error propagation, when the MCE-DFE was driven by noisy channel estimates.

Receiver output scattering plots of band-1 associated with the OMP, JB-SOMP, JB-MSSOMP, and JBT-MSSOMP algorithms are shown in Fig. 10 for the high SNR data. The best channel estimator, the JBT-MSSOMP algorithm, showed the best separated scattering plot and resulted in 4.11 dB gain in the output SNR over the OMP algorithm.

Finally, low density parity check code (LDPC) channel coding technology[30] was utilized. The coding rate was 2/3. The final BER in the decision-direct mode was provided in Table III and Table IV, for the high SNR data and low SNR data, respectively. In Table III, the BER obtained by OMP did not exhibit improvements after LDPC decoding, due to access errors. The receiver with the JBT-MSSOMP estimator

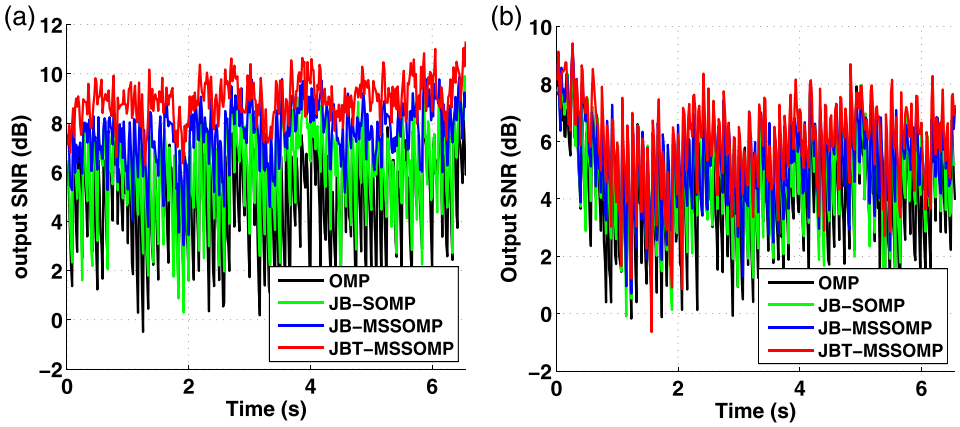

FIG. 9. (Color online) Output SNR in the decision-directed mode for the high SNR data (a) and the low SNR data (b) for band-1. The channel observation lengths in (a) and (b) were 16.67 and 26.67 ms, respectively.

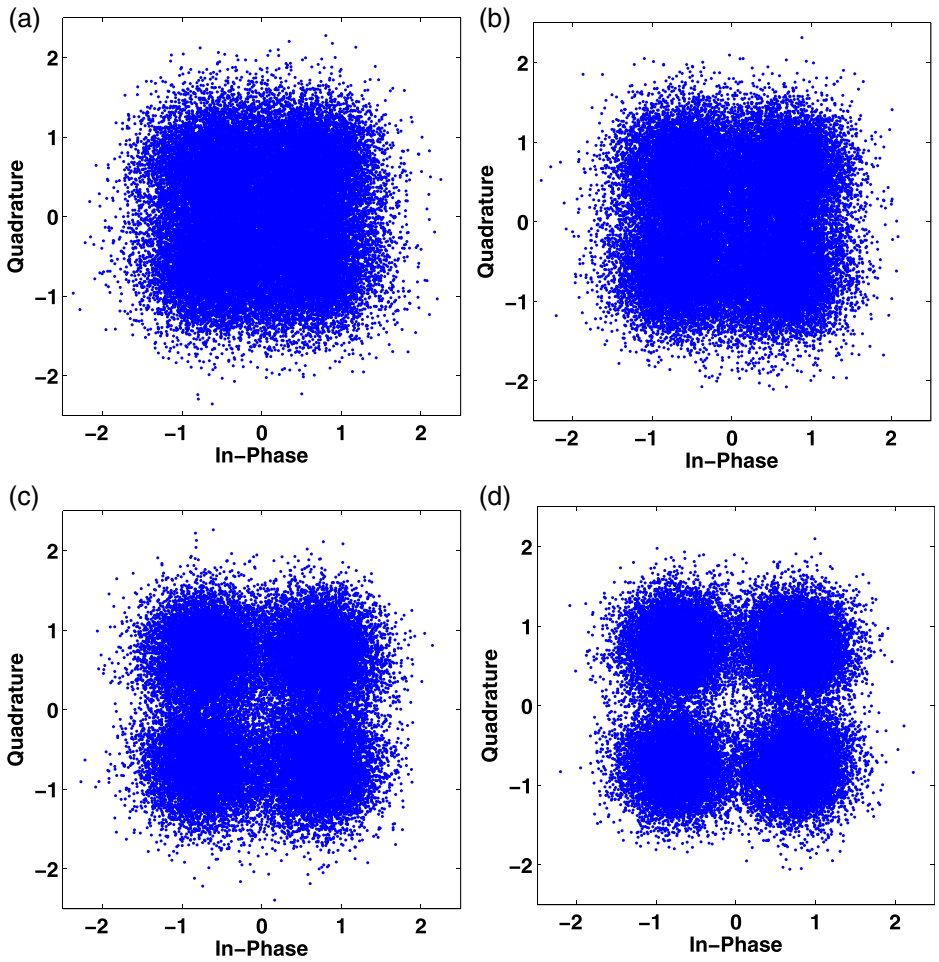

FIG. 10. (Color online) Constellations. (a)−(d) are the scatterplots from MCE-DFE obtained by the OMP, JB-SOMP, JB-MSSOMP, and JBT-MSSOMP algorithms, respectively, measured from high SNR data.

achieved zero error, after LDPC decoding. The LSQR channel estimation algorithm for MCE-DFE was failed in the working mode.

VI. CONCLUSIONS

The multiband underwater acoustic channels exhibit similar sparse structure in both adjacent data blocks and different sub-bands. In this paper, we applied DCS method that combined adjacent data blocks from each of sub-bands to improve the channel estimation performance under short observation length and low SNR. However, channels that contain differential tap delays will unavoidably degrade the performance of conventional DCS algorithm. To address the issue, we applied multiple selection strategy to joint band sparsity DCS channel estimation and joint both band and time sparsity DCS channel estimation, which were referred to as JB-MSSOMP and JBT-MSSOMP. The multiple selection strategy generates multiple candidates including channel delay candidates, channel coefficient candidates, and residual candidates, during each iteration. At last, the minimum residue is chosen to select the channel delays and coefficients. In this way, the estimation for common tap delays is enhanced, while the differential tap delays are correctly reconstructed. Simulation results indicated that, the proposed JB-MSSOMP and JBT-MSSOMP algorithms achieved about −1 dB and more than −2 dB average MSE than the OMP algorithm, respectively. Field experimental results indicated that, the JB-MSSOMP and JBT-MSSOMP algorithms

TABLE III. BER measured from high SNR data.

	OMP	JB-SOMP	JB-MSSOMP	JBT-MSSOMP
band-1				
Uncoded BER (%)	11.68	7.48	2.97	1.27
Coded BER (%)	11.25	3.40	0.00	0.00
band-2				
Uncoded BER (%)	15.52	9.77	4.50	2.17
Coded BER (%)	16.46	7.24	0.44	0.00
band-3				
Uncoded BER (%)	14.23	8.20	4.20	2.27
Coded BER (%)	13.43	4.76	0.42	0

TABLE IV. BER measured from low SNR data.

	OMP	JB-SOMP	JB-MSSOMP	JBT-MSSOMP
band-1				
Uncoded BER (%)	16.75	13.33	10.75	7.87
Coded BER (%)	16.58	12.72	9.29	3.40
band-2				
Uncoded BER (%)	16.35	12.18	10.52	7.73
Coded BER (%)	16.55	10.81	8.71	2.15
band-3				
Uncoded BER (%)	17.73	13.13	11.67	9.85
Coded BER (%)	17.73	12.23	10.23	6.75

obtained higher output SNR than OMP both in short observation length and low SNR. After LDPC channel decoding, the JB-MSSOMP and JBT-MSSOMP obtained lower BER than OMP.

ACKNOWLEDGMENTS

The authors are grateful for the funding of the National Nature Science Foundation of China (No. 11574258) in support of the present research. And they would like to thank the people who have contributed to this paper. Y.Z. thanks the China Scholarship Council (CSC) (No. [2015]3022) for fellowship support.

[1]S. Roy, T. M. Duman, V. McDonald, and J. G. Proakis, "High-rate communication for underwater acoustic channels using multiple transmitters and space−time coding: Receiver structures and experimental results," IEEE J. Oceanic Eng. **32**(3), 663–688 (2007).
[2]P. A. V. Walree and G. Leus, "Robust underwater telemetry with adaptive turbo multiband equalization," IEEE J. Oceanic Eng. **34**(4), 645–655 (2009).
[3]A. Song and M. Badiey, "Time reversal acoustic communication for multiband transmission," J. Acoust. Soc. Am. **131**(4), EL283–EL288 (2012).
[4]G. Leus and P. A. V. Walree, "Multiband OFDM for covert acoustic communications," IEEE J. Sel. Areas Commun. **26**(9), 1662–1673 (2008).
[5]W. Zeng and W. Xu, "Fast estimation of sparse doubly spread acoustic channels," J. Acoust. Soc. Am. **131**(1), 303–317 (2012).
[6]W. Li and J. C. Preisig, "Estimation of rapidly time-varying sparse channels," IEEE J. Oceanic Eng. **32**(4), 927–939 (2008).
[7]X. Jiang, W. Zeng, and X. Li, "Time delay and Doppler estimation for wideband acoustic signal multipath environments," J. Acoust. Soc. Am. **130**(2), 850–857 (2011).
[8]X. Jiang, T. Kirubarajan, and W. Zeng, "Robust sparse channel estimation and equalization in impulsive noise using linear programming," Signal Process. **93**(5), 1095–1105 (2013).
[9]H. C. Song and W. S. Hodgkiss, "Diversity combining for long-range acoustic communication in deep water," J. Acoust. Soc. Am. **132**(2), EL68–EL78 (2012).
[10]J. Huang, C. Berger, S. Zhou, and J. Huang, "Comparison of basis pursuit algorithms for sparse channel estimation in underwater acoustic OFDM," in *Proceedings of MTS/IEEE OCEANS Conference*, Sydney, Australia (May, 2010).
[11]Y. Zhou, F. Tong, and G. Zhang, "Distributed compressed sensing estimation of underwater acoustic OFDM channel," Appl. Acoust. **117**, 160–166 (2017).
[12]C. Berger, S. Zhou, J. C. Preisig, and P. Willett, "Sparse channel estimation for multicarrier underwater acoustic communication: From subspace methods to compressed sensing," IEEE Trans. Signal Process. **58**(3), 1708–1721 (2010).
[13]T. Kang and R. A. Iltis, "Iterative carrier frequency offset and channel estimation for underwater acoustic OFDM systems," IEEE J. Sel. Areas Commun. **26**(9), 1650–1661 (2008).
[14]D. Baron, M. F. Duarte, M. B. Wakin, S. Sarvotham, and R. G. Baraniuk, "Distributed compressed sensing," arXiv:0901.3403 (2005).
[15]X. He, R. Song, and W. P. Zhu, "Pilot allocation for distributed-compressed-sensing-based sparse channel estimation in MIMO-OFDM systems," IEEE Trans. Veh. Technol. **65**(5), 2990–3004 (2016).
[16]P. Cheng, Z. Chen, Y. Rui, Y. J. Guo, L. Gui, M. Tao, and Q. T. Zhang, "Channel estimation for OFDM systems over doubly selective channels: A distributed compressive sensing based approach," IEEE Trans. Commun. **61**(10), 4173–4185 (2013).
[17]X. Rao and V. K. N. Lau, "Distributed compressive CSIT estimation and feedback for FDD multi-user massive MIMO systems," IEEE Trans. Signal Process. **62**(12), 3261–3271 (2014).
[18]W. Ding, F. Yang, W. Dai, and J. Song, "Time−frequency joint sparse channel estimation for MIMO-OFDM systems," IEEE Commun. Lett. **19**(1), 58–61 (2015).
[19]Y. Zhou, W. Jiang, F. Tong, and G. Zhang, "Exploiting joint sparsity for underwater acoustic MIMO communications," Appl. Acoust. **116**, 357–363 (2017).
[20]S. Kwon, J. Wang, and B. Shim, "Multipath matching pursuit," IEEE Trans. Inf. Theory **60**(5), 2986–3001 (2014).
[21]B. Shim, S. Kwon, and B. Song, "Sparse detection with integer constraint using multipath matching pursuit," IEEE Commun. Lett. **18**(10), 1851–1854 (2014).
[22]W. U. Bajwa, J. D. Haupt, G. M. Raz, S. J. Wright, and R. D. Nowak, "Toeplitz-structured compressed sensing matrices," in *IEEE/SP 14th Workshop on Statistical Signal Processing*, 2007, Madison, WI (September, 2007).
[23]J. A. Tropp, A. C. Gilbert, and M. J. Strauss, "Simultaneous sparse approximation via greedy pursuit," in *IEEE International Conference on Acoustics, Speech, and Signal Processing* (2005), Vol. 5, pp. v/721–v/724.
[24]D. Sundman, S. Chatterjee, and M. Skoglund, "Methods for distributed compressed sensing," J. Sens. Actuator Networks **3**(1), 1–25 (2013).
[25]J. A. Tropp, A. C. Gilbert, and M. J. Strauss, "Algorithms for simultaneous sparse approximation. Part I: Greedy pursuit," Signal Process. **86**(3), 572–588 (2006).
[26]B. L. Sturm and M. G. Christiansen, "Comparison of orthogonal matching pursuit implementations," in *Proceedings of 20th European Signal Process Conference* (EUSIPCO), Bucharest, Romania (August, 2012).
[27]T. Blumensath and M. E. Davies, "Gradient pursuits," IEEE Trans. Signal Process. **56**(6), 2370–2382 (2008).
[28]J. C. Preisig, "Performance analysis of adaptive equalization for coherent acoustic communications in the time-varying ocean environment," J. Acoust. Soc. Am. **118**(1), 263–278 (2005).
[29]A. Song, M. Badiey, V. K. McDonald, and T. C. Yang, "Time reversal receivers for high data rate acoustic multiple-input−multiple-output communication," IEEE J. Oceanic Eng. **36**(4), 525–538 (2011).
[30]J. Huang, S. Zhou, and P. Willett, "Nonbinary LDPC coding for multicarrier underwater acoustic communication," IEEE J. Sel. Areas Commun. **26**(9), 1684–1696 (2008).